Statistics of Fano parameters in a mesoscopic billiard

2005 J. Phys. A: Math. Gen. 38 10819

(http://iopscience.iop.org/0305-4470/38/49/021)

INSTITUTE OF PHYSICS PUBLISHING JOURNAL OF PHYSICS A: MATHEMATICAL AND GENERAL

J. Phys. A: Math. Gen. **38** (2005) 10819–10828 doi:10.1088/0305-4470/38/49/021

Statistics of Fano parameters in a mesoscopic billiard

V Uski[1,2], F Mota-Furtado[1] and P F O'Mahony[1]

[1] Department of Mathematics, Royal Holloway, University of London, Egham, TW20 0EX Surrey, UK
[2] Department of Physics, University of Turku, 20014 Turku, Finland

E-mail: ville.uski@iki.fi

Received 30 June 2005, in final form 19 September 2005
Published 22 November 2005
Online at stacks.iop.org/JPhysA/38/10819

Abstract

We report on numerical calculations of the Fano parameters characteristic of non-symmetric resonance profiles in the electron transport through a waveguide attached to an irregular cavity. The distribution of Fano parameters is calculated for this chaotic scattering system with preserved time-reversal symmetry. We note the role played by the parametrization of the background conductance in comparing random matrix theory predictions for the Fano parameters with numerical or experimental data. Our calculated distribution agrees well with random matrix theory predictions.

PACS numbers: 05.45.Pq, 72.10.−d, 73.23.Ad

1. Introduction

Characterizing resonances in electron transport through mesoscopic cavities has been a subject of great interest in the last two decades [1]. In many cases, resonance profiles are well approximated by Lorentzians. As first pointed out by Fano [2], the line shape of an individual resonance may differ substantially from a Lorentzian profile due to interference between direct and indirect interaction pathways, giving rise to Beutler–Fano profiles. Such profiles have been observed in many different nuclear, atomic and molecular scattering experiments, and, very recently, also in mesoscopic electronic transport experiments [3, 4]. The occurrence of Beutler–Fano resonances is a direct indication that the electron transport is at least partially coherent and that there are both resonant (indirect) and non-resonant (direct) paths involved which interfere. The shapes of the resonance profiles reveal information on the degree of coherence and related phenomena [5, 6].

In this paper we study a chaotic scattering system composed of an electron waveguide connected to a mesoscopic cavity, as illustrated schematically in figure 1. The diameter of the cavity and of the waveguide is smaller than the phase-coherence length of the electron. This means that quantum interference plays an important role in the electron transport through this

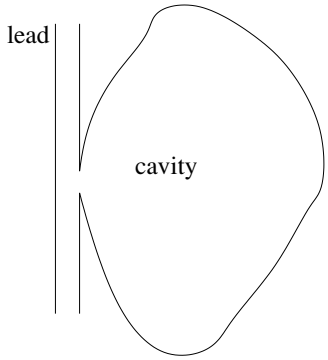

Figure 1. Schematic illustration of the system studied.

system, which is manifested in the occurrence of the Beutler–Fano resonance profiles. We neglect absorption, inelastic scattering and interaction effects, and concentrate on the coherent electron transport. We calculate the conductance as a function of energy and hence, through a fitting procedure, we extract the Fano q parameter and the width for each resonance in a given energy interval. We thus obtain the probability distribution for the q-parameter in the same way as an experimentalist would extract the distribution from their data. To obtain reliable statistics we in practice use the Anderson localization model to simulate the cavity which enables us to average over the disorder as opposed to the energy.

Recently, the statistics of the Beutler–Fano profiles were studied analytically [7, 8] both for chaotic scattering systems and for atomic and molecular photoexcitation [14, 15]. For scattering systems the predicted q distribution [7] is based on a random matrix theory (RMT) of the quantum transport [9], where the indirect pathways are assumed to cover ergodically the internal system, as is the case in classically chaotic quantum systems [10, 11]. We compare the numerically determined q distribution for our system, which should be typical of that for a chaotic scattering system, with that derived from RMT. We find that the numerically determined distribution is strongly influenced by the difficulty in finding resonances with very narrow widths, a feature shared by any actual experiment. We show how this difficulty can be taken into account in the RMT theory by introducing an effective cut-off value for the smallest widths, and we discuss the implications of our findings with respect to comparing RMT with real experimental data for the q distribution. We find good agreement with the RMT predictions.

The paper is organized as follows. In section 2, we briefly outline the theory used. In section 3, we present the numerical procedure and give the details of the specific model we have used. In section 4 we discuss our numerical results, and finally give the conclusions in section 5.

2. Theory

Electron transport through the system illustrated in figure 1 gives rise to Beutler–Fano resonance profiles due to the interference between 'resonant' and 'non-resonant' transmission paths along the waveguide. The resonant paths enter the cavity and explore it ergodically before re-entering the waveguide. The non-resonant paths, on the contrary, pass the cavity or enter it for a time shorter than the ergodic time. The transmission amplitude t can be written as a sum of the resonant and non-resonant contributions $t = t_r + t_n$. The resonant

contribution t_r is determined by the coupling of the discrete energy levels of a closed cavity and the continuum spectrum of the waveguide [9]. Due to the coupling, the discrete energy levels become resonances with Lorentzian profiles. Near each resonance energy E_0 the resonant transmission amplitude can be expressed as

$$t_r = \frac{z_r \Gamma}{2(E - E_0) + \mathrm{i}\Gamma}, \tag{1}$$

where Γ is the resonance width and z_r is an excitation amplitude. z_r gives the peak amplitude for the transmission in the absence of direct transmission, i.e., it is related to the probability of exciting a particular resonance in the cavity.

The non-resonant contribution t_n is independent of the discrete energy levels of the cavity, and is therefore a slowly varying function of energy. By assuming that it is a constant over the resonance region, one obtains the Beutler–Fano form

$$g(E) = |t|^2 = |t_n|^2 \frac{|2(E - E_0) + q\Gamma|^2}{4(E - E_0)^2 + \Gamma^2}, \tag{2}$$

where $g(E)$ is the dimensionless conductance, and

$$q = \mathrm{i} + z_r / t_n \tag{3}$$

is the Fano parameter. The fluctuations in q are therefore dependent on the fluctuations in z_r.

For simplicity, we restrict our attention to the energy regime where only one channel is open, i.e., there is only one propagating mode in the waveguide. In this case, the scattering matrix S is a 2×2 matrix:

$$S = \begin{pmatrix} r' & t \\ t' & r \end{pmatrix}, \tag{4}$$

where r', t' (r, t) are the reflection and transmission amplitudes of an electron coming from the 'upper' ('lower') arm of the waveguide.

To make a connection with RMT the authors in [7] parameterize the S matrix by decomposing it into resonant and non-resonant parts. The non-resonant part is given by the average scattering matrix $\bar{S}$. It can be written in terms of its polar decomposition:

$$\bar{S} = U\sqrt{1 - T}U^T, \tag{5}$$

where U is a 2×2 unitary matrix and $T = \mathrm{diag}(T_1, T_2)$. The parameters T_1 and T_2 are called the sticking probabilities [12], and they represent the probability of the electron to enter the ergodic paths from the 'eigenmodes' given by the columns of the matrix U. $\bar{S}$ is here assumed to be symmetric, which is always true in the case of preserved time-reversal symmetry. $\bar{S}$ is a subunitary matrix, which is a sum of the contributions from the direct paths passing the cavity.

The remaining, resonant part of the scattering matrix is written as follows:

$$\delta S = S - \bar{S} = U\sqrt{T}\frac{1}{1 + S_0\sqrt{1 - T}} S_0 \sqrt{T} U^T \tag{6}$$

where S_0 represents the scattering matrix of the cavity.

Representing S_0 in terms of its Green function, and assuming $T_1, T_2 \ll 1$ which justifies the assumption that the resonances are narrow and well separated, it was shown in [7] that the S-matrix near an isolated resonance can be written as

$$S = \bar{S} + \delta S, \tag{7}$$

where $\bar{S} \simeq UU^T$ and

$$\delta S(\varepsilon) = -U\frac{2\mathrm{i}\Delta\sqrt{T}\psi^\dagger\psi\sqrt{T}}{4\pi\varepsilon + \mathrm{i}2\pi\Gamma}U^T. \tag{8}$$

$\varepsilon = E - E_0$ measures the energy from the resonance position and $\psi = (\psi_1, \psi_2)$, where ψ_i are the wave-function amplitudes at the contact between the waveguide and the cavity. Δ is mean level spacing.

Assuming that both ψ_1 and ψ_2 are normally distributed for a chaotic system, one can use RMT to derive the distribution of q parameters from the above expression for the S-matrix (see [7]). The type of statistics found will depend on the time-reversal symmetry (TRS) of the system. We confine our attention here to systems with TRS, for which the Fano parameters are real numbers. Following the notation of [7], we use the 'normalized' q-parameters, $\tilde{q} = q/q_{\max}$, where $q_{\max} = \sqrt{|t_n|^{-2} - 1}$. The RMT predicted distribution for the q parameter is

$$P(\tilde{q}) = \frac{1}{\pi}\sqrt{\frac{1+\alpha}{1-\tilde{q}^2}}\,\frac{1+\alpha(1-\tilde{q}\tilde{q}_a)/2}{1+\alpha(1-\tilde{q}\tilde{q}_a)+\alpha^4(\tilde{q}-\tilde{q}_a)^2/4}, \tag{9}$$

where $\alpha = T_2/T_1 - 1$, $q_a = \tilde{q}_a q_{\max}$, with

$$q_a = \mathrm{i}(U_{11}U_{21} - U_{22}U_{12})/(U_{11}U_{21} + U_{22}U_{12}). \tag{10}$$

q_a is a real number due to the unitarity of U and represents the typical q, i.e., it is the position of the maximum in the distribution of q parameters. T_1 and T_2 are chosen to be in ascending order, $T_2 \geqslant T_1$. $q_{\max}$ is the maximum possible value of q, given the constraint for the conductance, $g \leqslant 1$, in the case of a single open channel. Equation (9) is obtained after integrating over the distribution of the resonance widths Γ, which also fluctuate according to RMT.

Equation (9) is valid only if $T_1, T_2 \ll 1$, i.e., when the opening to the cavity is small compared to the width of the waveguide. This not only ensures that the resonances do not overlap, but it is also important in the derivation of equation (7), where it is assumed that $\bar{S}$ can be expressed without the sticking probabilities, i.e., $\bar{S} \simeq UU^T$.

The width of a resonance depends on the sticking probabilities and the wavefunction amplitudes such that $\Gamma = \Gamma_1|\psi_1|^2 + \Gamma_2|\psi_2|^2$, where $\Gamma_i = T_i\Delta/(2\pi)$. Assuming the amplitudes are Gaussian distributed, one obtains the distribution of the widths in the presence of TRS [7] as

$$P(\Gamma) = \tfrac{1}{2}(\Gamma_1\Gamma_2)^{-1/2}\exp(-\Gamma/4\Gamma_1)\exp(-\Gamma/4\Gamma_2)I_0(\Gamma|\Gamma_1 - \Gamma_2|/4\Gamma_1\Gamma_2), \tag{11}$$

where I_0 is the modified Bessel function. Note that if $\Gamma_1 = \Gamma_2$ this expression reduces to the well-known χ^2 distribution for the widths.

2.1. The average scattering matrix $\bar{S}$

In order to interpret our numerical results, we briefly discuss the possible parameter values given by the polar decomposition of $\bar{S}$. As $T_1, T_2 \ll 1$, and $\bar{S} \simeq UU^T$ we can write U as

$$U = \begin{pmatrix} \exp(\mathrm{i}\alpha)\cos\gamma & \exp(\mathrm{i}\beta)\sin\gamma \\ -\exp(-\mathrm{i}\beta)\sin\gamma & \exp(-\mathrm{i}\alpha)\cos\gamma \end{pmatrix}. \tag{12}$$

This is a general form of a 2×2 unitary matrix with determinant equal to unity. More generally, the matrix elements can have an additional phase factor, which we can omit here without loss of generality.

One obtains

$$q_a = \cot(\alpha - \beta) \tag{13}$$

$$q_{\max}^2 = (1 - \sin^2 2\gamma \sin^2(\alpha - \beta))/(\sin^2 2\gamma \sin^2(\alpha - \beta)). \tag{14}$$

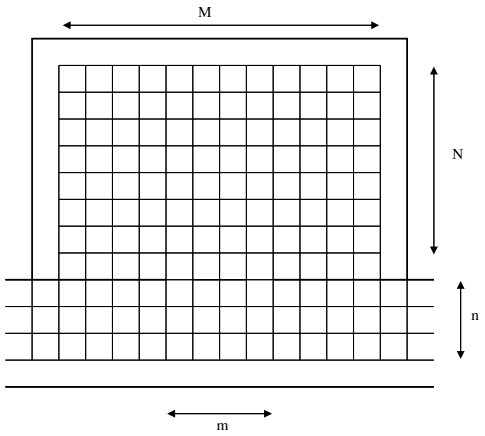

Figure 2. The system is composed of a rectangular cavity with an opening to an infinitely long electron waveguide. The geometry is discretized by a regular square lattice with $m \times n + M \times N$ lattice sites. m is the number of sites connecting the cavity and the waveguide. Each lattice point is associated with an on-site potential ε_k and each connection between the points by a hopping parameter $V_{kk'}$.

We remark that if $\cos\gamma = \sin\gamma \Rightarrow \gamma = \pi/4$, then $q_{\max} = q_a$, i.e., the maximum q equals the typical q. This happens when $|\bar{S}_{12}|^2 = 1$, that is, when $\bar{S}$ is a scattering matrix of a waveguide with one open channel (without the cavity). In that case, $\alpha - \beta = \pm\pi/2$. If the waveguide includes a *small* hole to the cavity, then one expects that still $|\bar{S}_{12}|^2 \simeq 1$, and $q_a \simeq q_{\max}$. Our numerical results show that this is indeed what happens.

3. The model and the calculation of the S matrix

We approximate the Hamiltonian H of our system with the help of the tight-binding representation:

$$H = \sum_k \varepsilon_k c_k^\dagger c_k + \sum_{kk'} V_{kk'} c_k^\dagger c_{k'}, \tag{15}$$

where the subscripts k denote the sites of a square lattice covering the geometry, as illustrated in figure 2. $c_k^\dagger$ and c_k are the creation and annihilation operators, corresponding to each site, and ε_k is the potential energy. The hopping parameters $V_{kk'}$ are set equal to the energy unit, if k and k' denote the nearest-neighbour sites. Otherwise, $V_{kk'}$ are zero.

The on-site potentials ε_k are constant outside the cavity, i.e., inside the wave guides. We set this constant to 4 such that the lower band edge lies at $E = 0$, when $W = 0$. Inside the cavity, ε_k are uniformly distributed in the range $[4 - W/2, 4 + W/2]$. The cavity is actually modelled by the Anderson model of localization [13], which is known to show universal statistics for the energy levels and wave functions, when W is chosen in the diffusive regime, below the localization threshold. Alternatively, the cavity could be modelled by an irregular billiard, where the electron propagates ballistically. The advantage of the Anderson model is that it is possible to compute the statistics from arbitrarily many samples, each having different random potentials. It also allows us to apply a simple rectangular geometry.

The reflection and transmission amplitudes, and hence the S matrix, are calculated from the matrix elements of Green's function $G = (E - H)^{-1}$ as follows [17]:

$$r' = -[1 - \mathrm{i}2\sin\theta\langle 1|\mathbf{G}_{00}|1\rangle] \tag{16}$$

$$t' = \mathrm{i}2\sin\theta\langle 1|\mathbf{G}_{01}|1\rangle \tag{17}$$

$$r = -[1 - \mathrm{i}2\sin\theta\langle 1|\mathbf{G}_{11}|1\rangle] \tag{18}$$

$$t = \mathrm{i}2\sin\theta\langle 1|\mathbf{G}_{10}|1\rangle, \tag{19}$$

where $\sin\theta = \sqrt{E - 2(1 - \cos[\pi/(n+1)])}$. $\mathbf{G}_{00}$, $\mathbf{G}_{01}$, $\mathbf{G}_{10}$ and $\mathbf{G}_{11}$ denote $n \times n$ blocks of the full Green's function matrix. $\mathbf{G}_{00}$ ($\mathbf{G}_{11}$) contains all the matrix elements $G_{kk'}$ with site indices k, k' of a single column in the left (right) arm of the waveguide. $\mathbf{G}_{01}$ and $\mathbf{G}_{10}$ contain the elements corresponding to transmission between the two columns on the left and right arms. The brackets $\langle 1|\cdot|1\rangle$ denote the matrix elements in the mode basis. For example,

$$\langle 1|\mathbf{G}_{00}|1\rangle = \sum_{j,j'=1}^{n} \phi_1(j)\phi_1(j')(\mathbf{G}_{00})_{jj'}, \tag{20}$$

where ϕ_1 is the first transversal mode in the waveguide. The modes are given by [17]

$$\phi_\alpha(j) = A_\alpha \sin[(\alpha\pi j)/(n+1)] \tag{21}$$

$$A_\alpha = \left\{ \frac{j}{2} + \frac{1}{2}\,\mathrm{Re}\left[\frac{1 - \exp(\mathrm{i}2\pi\alpha n/(n+1))}{1 - \exp(-\mathrm{i}2\pi\alpha/(n+1))} \right] \right\}^{-1/2} \tag{22}$$

for $\alpha = 1, \ldots, n$.

To obtain G for the tight-binding lattice, we have applied the tight-binding Green function technique, described in [17]. In this case, we separately computed the matrix elements for Green's function of the waveguide and that of the cavity, and applied Dyson's equation to obtain the matrix elements of the full Green function. For the cavity Green function, only those matrix elements with site indices at the opening of the cavity are needed, which greatly reduces the set of linear equations to be solved.

4. Results

We selected a suitably narrow energy interval $[E - \delta E/2, E + \delta E/2]$ such that the interval lies between the first and second threshold energies, E_1 and E_2, where [17]

$$E_i = 2(1 - \cos((n - i + 1)\pi/(n+1))). \tag{23}$$

n is the width of the waveguide. By using a simple loop over seeds of the random number generator, we looked for those realizations of the model, which have a resonance inside the chosen energy interval, with $\delta E \ll \Delta$, the mean level spacing. To ensure that there is no sample-to-sample fluctuation in the direct transmission and reflection amplitudes and, hence, $\bar{S}$, the realizations were chosen such that the on-site potentials near the opening of the cavity are always the same, i.e., they only fluctuate from site to site but not from sample to sample. We can control the size of the sticking probabilities T_1 and T_2 by varying the size of the opening to the cavity.

The resonance widths Γ and positions E_0 were determined by fitting the total phase shift sum [18] by

$$\delta(E) = \arctan\left(\frac{E - E_0}{\frac{1}{2}\Gamma} \right) + \delta_{\mathrm{bg}}(E), \tag{24}$$

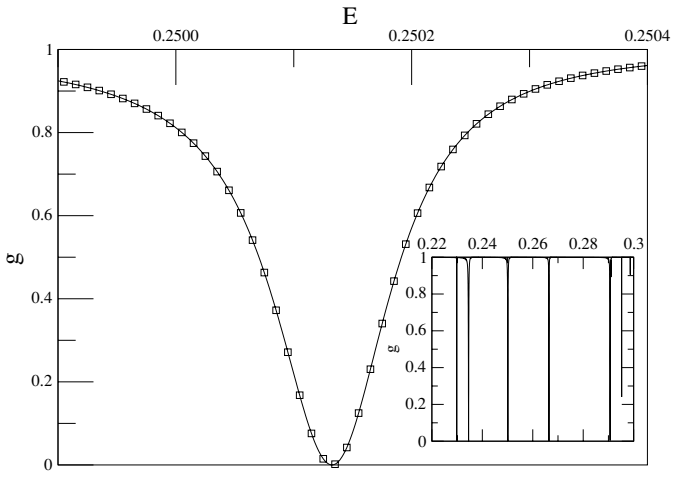

Figure 3. An example of a resonance in one realization of the model. The rectangles show the computed values of conductance g at different energies, and the solid line shows a fit of the Beutler–Fano form. The fit gives the value of the Fano parameter q. The inset shows several resonances at nearby energies.

where the background phase shift $\delta_{bg}(E)$ was approximated by a second-order polynomial. The phase shifts δ_i are determined by the eigenvalues $\exp(2i\delta_i)$ of the scattering matrix S, whose matrix elements r', t', r and t are computed as described in section 3. The q parameters were then obtained by fitting the Beutler–Fano function, equation (2), to the calculated conductance data for each realization. An example of such fitting is shown in figure 3. The conductance is obtained from the off-diagonal elements of the S-matrix, $g(E) = |t|^2 = |t'|^2$.

For a system defined by $n = 10, m = 3, N = 53, M = 20, E = 0.25$ and $W = 1.0$ we calculated the scattering matrix S for many ($\sim 10^7$) realizations of the disorder potential, and hence obtained $\bar{S}$ the average S-matrix. In order to make sure that the parameters of our model lie in the right regime for RMT to apply, we checked that the statistics of the eigenfunctions of the Hamiltonian corresponding to the closed cavity follows the universal statistics described by RMT. It is known that the wave-function amplitudes should follow the Porter–Thomas distribution [19] in the presence of the TRS. We verified that this condition is very accurately fulfilled for our system (see figure 4). As a further check, we calculated histograms for the fluctuating part δS of the scattering matrix. This is obtained by subtracting $\bar{S}$ from the full scattering matrix S. δS is given by equation (6), where U, T_1, T_2 are obtained from the decomposition of $\bar{S}$. According to RMT, the matrix S_0 represents uniformly distributed symmetric unitary 2×2 matrices (circular orthogonal ensemble [9]). Figure 5 shows that this requirement is fulfilled in our system. We remark that the distributions are not centred at zero, even though the ensemble average of δS vanishes due to the asymmetry of the distributions.

As shown earlier q_a and q_{max} can typically be very similar for the model we use. q_a can be made smaller than q_{max} by adding a potential barrier inside the waveguide such that the random potential inside the cavity is extended from the opening to the opposite wall of the waveguide, the width of the barrier being equal to m. This enhances the direct reflection, reducing the sticking probabilities and the resonance widths.

We calculate many thousands of resonances and fit each of them to obtain the width Γ and Fano parameter q for each of them. We show in figure 6 a histogram of the calculated

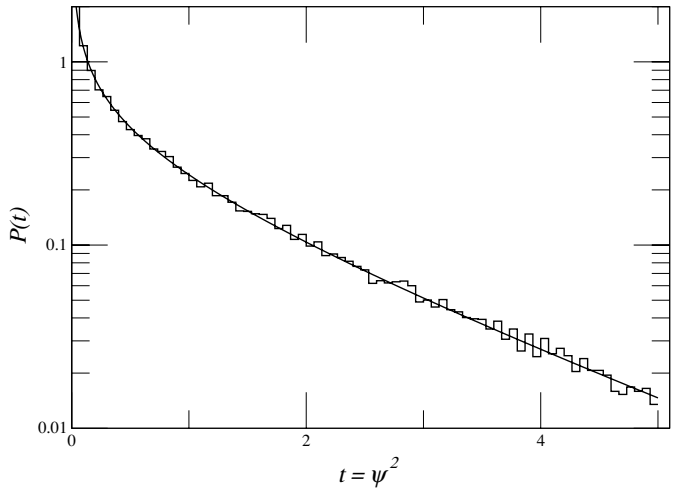

Figure 4. Histogram of the wave function intensities for the same system as in figure 7. The smooth line shows the Porter–Thomas distribution $\exp(-t/2)/\sqrt{2\pi t}$.

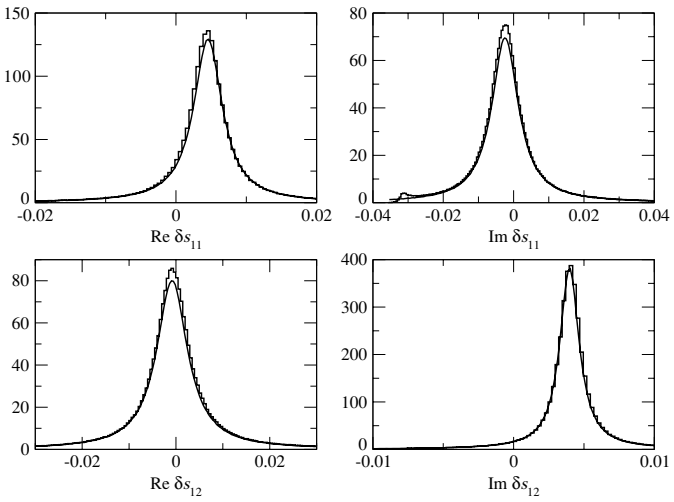

Figure 5. Histograms of the fluctuations of the scattering matrix elements for the same system as in figure 7. The solid lines show the corresponding distributions according to the RMT. They were determined numerically by sampling S_0 over the circular ensemble.

distribution of widths. It is apparent by the drop near zero that very small widths are largely absent. This is so partly due to the finite resolution of the resonance searching algorithm, and partly due to the difficulty in calculating the S matrix near the poles in the complex energy plane (Γ gives the imaginary part of the pole). We can estimate a cut-off Γ_c from the histogram of the widths shown in figure 6, $\Gamma_c \sim 1.9 \times 10^{-5}$, below which we cannot go. In a real conductance experiment a similar situation would arise as it would not be possible to resolve resonances below a certain width. We will use this cut-off value Γ_c below to determine the RMT distribution for the q parameter in the presence of a cut-off.

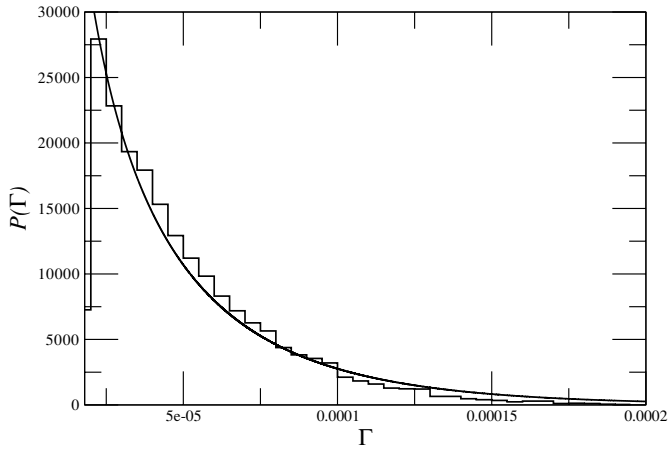

Figure 6. Histogram of the resonance widths. The smooth line shows equation (11) with $\Gamma_1 \sim 1.2 \times 10^{-6}$ and $\Gamma_2 \sim 2.5 \times 10^{-5}$. These values give the same $\alpha = \Gamma_2/\Gamma_1 - 1$ as in figure 7.

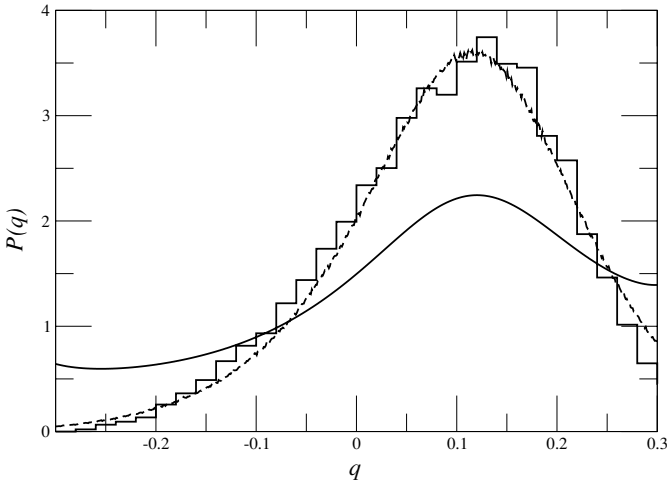

Figure 7. Histogram of the Fano parameters for a system with a geometry $3 \times 10 + 53 \times 20$ and with a narrow potential barrier inside the waveguide. The solid smooth line shows equation (9) with parameters $\alpha = 20, q_a = 0.107, q_{max} = 0.36$. The dashed line shows the numerically calculated RMT distribution with an effective cut-off $\Gamma_c \sim 1.9 \times 10^{-5}$.

To compare the calculated distribution with the RMT prediction in equation (9) we need to calculate T_1, T_2, q_a and q_{max}. $\bar{S}$ is calculated by averaging the S matrix over the very large ensemble we have used. The polar decomposition of $\bar{S}$ gives U and T_1 and T_2, and hence q_a and q_{max}. The maximum value, q_{max}, can be calculated easily from $\bar{S}$, giving the value $q_{max} \simeq 0.360$ which agrees well with the numerical values for q. The parameter α is equal to 20. One additional parameter, namely Γ_2 still needs to be determined. We used the formula $\Gamma_2 = T_2\Delta/(2\pi)$, where T_2 the sticking probability was obtained from the decomposition of $\bar{S}$ and Δ is the mean level spacing from the eigenenergy spectrum of the closed cavity. The obtained value, $\Gamma_2 \sim 2.5 \times 10^{-5}$, is consistent with the Γ histogram, too. So, two independent checks give the same value for Γ_2.

We show in figure 7 the histogram of computed values for the q distribution and compare it with the RMT prediction from equation (9) assuming no cut-off in the width distribution. We notice that the central peak lies much lower than in the histogram and the tails decay more slowly. The dashed line in figure 7 shows the q distribution resulting from assuming that there is an effective cut-off Γ_c for narrow resonances, that is, all the resonances with $\Gamma < \Gamma_c$ are omitted in the RMT ensemble. To calculate the RMT distribution with a cut-off, we used equation (8) and took the amplitudes ψ_1 and ψ_2 randomly from a normal distribution. Then we calculated Γ and q from ψ_1 and ψ_2 for given α and U using the formulae given in section 2. We thus calculated the RMT distribution of q values, excluding those resonances with $\Gamma < \Gamma_c$. We checked that this gives the analytic distribution given by equation (9) when we take $\Gamma_c = 0$. As can be seen from figure 7 the RMT distribution with a cut-off agrees very well with the numerically determined q distribution showing that it is important to incorporate the effect of the missing resonances in the statistics.

5. Conclusions

We have studied numerically the distribution of Fano q parameters for a chaotic scattering system by extracting the widths and q parameters from the calculated conductance. We have checked that our model satisfies the main criteria assumed in RMT and we have compared the numerical q distribution for a system with TRS to the theoretical predictions from RMT. The RMT prediction depends on a set of parameters related to the background conductance. These have been determined and very good agreement is obtained between the RMT theory and the calculated distribution when a cut-off is introduced to eliminate resonances with very small widths. A similar cut-off would exist in any real experimental situation as one would not be able to resolve the smallest widths.

Acknowledgment

This work was supported by the European Research Training Network QTRANS.

References

[1] Verbaarschot J J M, Weidenmuller H A and Zirnbauer M R 1985 *Phys. Rep.* **129** 367
[2] Fano U 1961 *Phys. Rev.* **124** 1866
[3] Göres J, Goldhaber-Gordon D, Heemeyer S and Kastner M A 2000 *Phys. Rev.* B **62** 2188
[4] Kobayashi K, Aikawa H, Sano S, Katsumoto S and Iye Y 2004 *Phys. Rev.* B **70** 035319
[5] Rotter S, Libisch F, Burgdörfer J, Kuhl U and Stöckmann H-J 2004 *Phys. Rev.* E **69** 046208
[6] Persson E, Rotter I, Stöckmann H-J and Barth M 2000 *Phys. Rev. Lett.* **85** 2478
[7] Clerk A A, Waintal X and Brouwer P W 2001 *Phys. Rev. Lett.* **86** 4636
[8] Ihra W 2002 *Phys. Rev.* A **66** 020701(R)
[9] Beenakker C W J 1997 *Rev. Mod. Phys.* **69** 731
[10] Stöckmann H-J 1999 *Quantum Chaos: Introduction* (Cambridge: Cambridge University Press)
[11] Casati G and Chirikov B 1995 *Quantum Chaos Between Order and Disorder* (Cambridge: Cambridge University Press)
[12] Iida S, Weidenmüller H A and Zuk J A 1990 *Ann. Phys., NY* **200** 219
[13] Anderson P W 1958 *Phys. Rev.* **109** 1492
[14] Alhassid Y, Fyodorov Y V, Gorin T, Ihra W and Mehlig B 2003 *Preprint* cond-mat/0309521
[15] Gorin T, Mehlig B and Ihra W 2004 *J. Phys. A: Math. Gen.* **37** L345
[16] Luttinger J M 1951 *Phys. Rev.* **84** 814
[17] Sols F, Macucci M, Ravaioli U and Hess K 1989 *J. Appl. Phys.* **66** 3892
[18] Busby D W, Burke P G, Burke V M, Noble C J and Scott N S 1998 *Comput. Phys. Commun.* **114** 243
[19] Porter C E and Thomas R G 1956 *Phys. Rev.* **104** 483